Estimating the reproduction number and transmission heterogeneity from the size distribution of clusters of identical pathogen sequences

Cécile Tran-Kiem[1], Trevor Bedford[1,2]

1. Vaccine and Infectious Diseases Division, Fred Hutchinson Cancer Center, Seattle, WA, USA
2. Howard Hugues Medical Institute, Seattle, WA, USA

Correspondence should be addressed to Cécile Tran-Kiem (ctrankie@fredhutch.org).

Abstract

Quantifying transmission intensity and heterogeneity is crucial to ascertain the threat posed by infectious diseases and inform the design of interventions. Methods that jointly estimate the reproduction number R and the dispersion parameter k have however mainly remained limited to the analysis of epidemiological clusters or contact tracing data, whose collection often proves difficult. Here, we show that clusters of identical sequences are imprinted by the pathogen offspring distribution, and we derive an analytical formula for the distribution of the size of these clusters. We develop and evaluate a novel inference framework to jointly estimate the reproduction number and the dispersion parameter from the size distribution of clusters of identical sequences. We then illustrate its application across a range of epidemiological situations. Finally, we develop a hypothesis testing framework relying on clusters of identical sequences to determine whether a given pathogen genetic subpopulation is associated with increased or reduced transmissibility. Our work provides new tools to estimate the reproduction number and transmission heterogeneity from pathogen sequences without building a phylogenetic tree, thus making it easily scalable to large pathogen genome datasets.

Significance statement

For many infectious diseases, a small fraction of individuals has been documented to disproportionately contribute to onward spread. Characterizing the extent of superspreading is a crucial step towards the implementation of efficient interventions. Despite its epidemiological relevance, it remains difficult to quantify transmission heterogeneity. Here, we present a novel inference framework harnessing the size of clusters of identical pathogen sequences to estimate the reproduction number and the dispersion parameter. We also show that the size of these clusters can be used to estimate the transmission advantage of a pathogen genetic variant. This work provides crucial new tools to better characterize the spread of pathogens and evaluate their control.

Introduction

Characterizing transmission parameters describing the intensity and heterogeneity of infectious diseases' spread is fundamental both to understand the threat posed by epidemics and to inform their control. The reproduction number R, which describes the average number of secondary infections engendered by a single primary case, is a key statistic as it directly reflects the ability for a pathogen to propagate within a population (corresponding to R > 1) (1–4). Additionally, heterogeneity in the contribution of individuals to disease spread has important implications for outbreak control. When a small proportion of individuals plays a disproportionate role in transmission, control strategies targeting these *superspreaders* can largely reduce the epidemic burden with a small effort (1,5). Individual variation is typically measured with the dispersion parameter k, with lower values corresponding to a higher degree of heterogeneity (5).

Estimates of R can be obtained from the analysis of epidemiological time series (*e.g.* cases, hospitalizations or deaths). These methods have widely been used to track in real-time changes in

transmission rates or the impact of interventions (2,6,7). However, these approaches do not allow the estimation of the dispersion parameter k. Other methods have been proposed to jointly infer the reproduction number and the dispersion parameter from transmission chain data or epidemiological cluster sizes (5,8–10). The collection of such data relies on the identification of epidemiological relationships between infected individuals. This can however prove difficult if there is widespread community transmission (hindering our ability to identify the putative infector), if a fraction of infected individuals remains undetected or if the resources available for such investigation remain scarce.

Pathogen genome sequences can provide insights into the proximity of individuals in a transmission chain (11–13) or into the epidemiological processes associated with their spread (14). Phylodynamic approaches have been widely used to estimate epidemiological parameters from the shape of phylogenies, including the reproduction number R (15–18). Current methods however face a number of limitations. First, they require intensive computation and therefore do not scale well to large datasets. New approaches to estimate transmission parameters from sequence data without resorting to subsampling are hence of primary interest. Second, they generally do not enable to estimate the extent of transmission heterogeneity (superspreading or k). Finally, polytomy-rich phylogenies tend to decrease the statistical power available to estimate growth rates, thus deprecating the value of these methods during the early stage of an outbreak or when large superspreading events occur.

Here, we demonstrate that the size distribution of clusters of identical sequences (or of polytomies) is shaped by epidemic transmission parameters (R and k). We develop and evaluate a statistical model accounting for heterogeneity in transmission to estimate the reproduction number R and the dispersion parameter k from this distribution. Our method does not require building the associated phylogenetic tree. Applying our framework to different epidemiological situations, we recover expected transmission parameters for well-characterized pathogens. Finally, we develop a novel inference framework to quantify differences in the transmissibility of genetic variants.

Results

Distribution of the number of offspring with identical genomes

In this work, we used the formalism introduced by Lloyd-Smith et al. (5) and assumed that the number of secondary cases (or offspring) generated by a single index case follows a negative binomial distribution of mean R (the reproduction number) and dispersion parameter k. We focused here on the spread of a pathogen that mutates. More specifically, we were interested in the number of offspring who are infected by a pathogen characterized by having the same genome sequence as their infector. We introduced p, the probability that a transmission event occurs before a mutation event, and we showed that the number of offspring with identical genomes follows a negative binomial distribution of mean $p\,R$ and dispersion parameter k (see Materials and methods). This highlights that the relative timescale at which mutation and transmission events typically occur (captured by p, Figure 1A) along with transmission intensity (captured by R), will shape the expected mean number of secondary cases with identical sequences. For example, assuming the mean waiting time until a mutation event is three times that the waiting time to a transmission event, the mean number of offspring with identical genomes would be respectively 0.6, 0.75 and 0.9 for R of 0.8, 1.0 and 1.2. These values would drop to 0.2, 0.25 and 0.3 assuming the mean waiting time until mutation is a third that until transmission (Figure 1B).

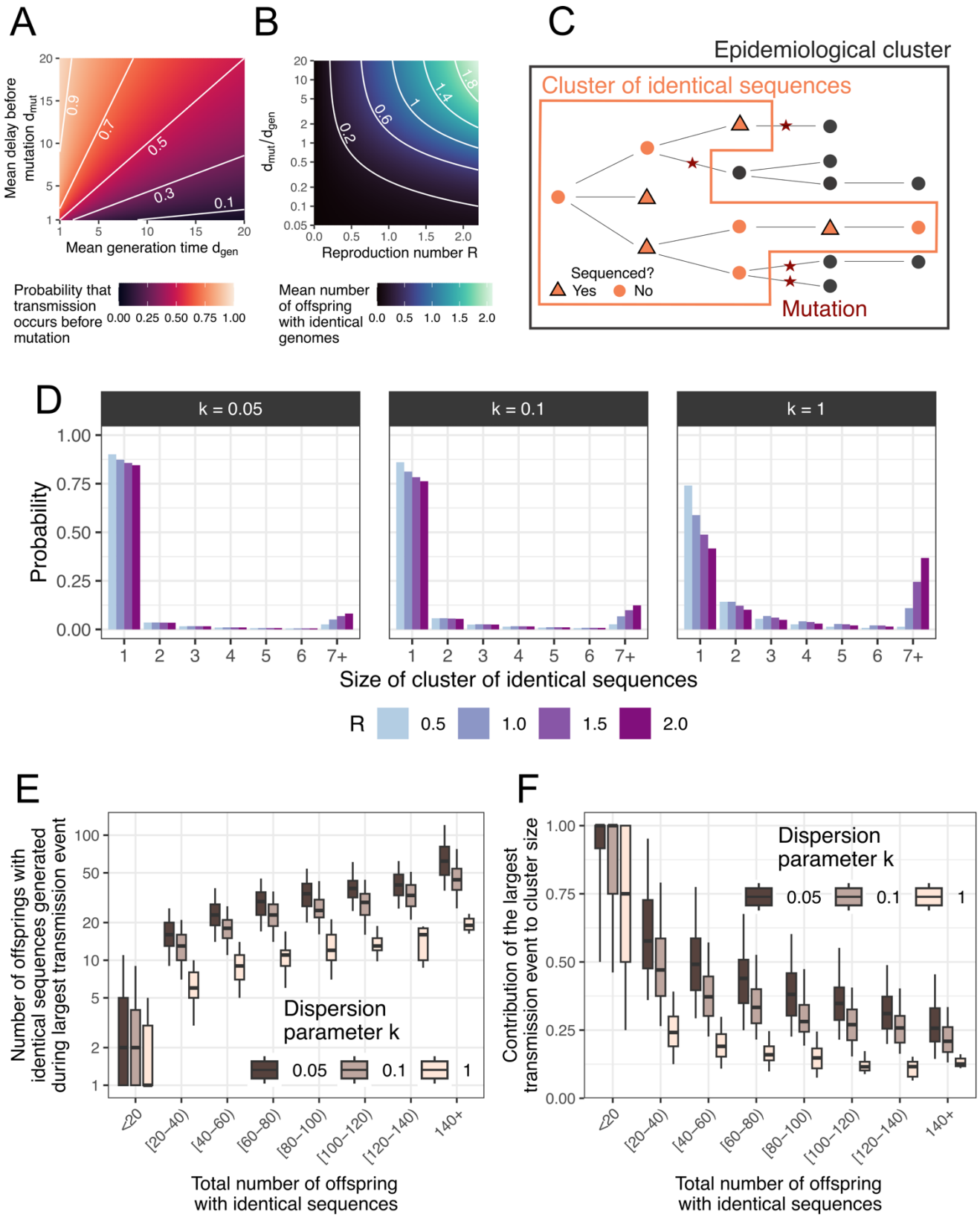

Figure 1: Impact of the reproduction number R and the dispersion parameter k on the size distribution of clusters of identical sequences. A. Probability that transmission occurs before mutation

as a function of the mean generation time d_{gen} and the mean delay before the occurrence of a mutation d_{mut}. **B.** Mean number of offspring with identical genomes as a function of the reproduction number and the ratio of the average delay before the occurrence of a mutation d_{mut} and the average delay between generations d_{gen} **C.** Relationship between epidemiological clusters and clusters of identical sequences. **D.** Probability mass function of the size of clusters of identical sequences for different values of R and k and assuming a probability that transmission occurs before mutation of 0.7. **E.** Number of offspring with identical sequences generated during the largest transmission event as a function of the total number of offspring with identical genomes generated by a primary case exploring different values for k. **F.** Contribution of the largest transmission event to the total number of offspring with identical sequences as a function of the total number of offspring with identical genomes generated by a primary case exploring different values for k. In E-F, we report for each value of k the results of 100,000 simulated clusters of identical sequences with a reproduction number R of 1 and a probability that transmission occurs before mutation of 0.7. In E-F, the boxplots indicate the median along the 5%, 25%, 75% and 95% quantiles. In E-F, the total number of offspring with identical sequences is equal to the size of a cluster of identical sequences minus 1. In A-B, we assume that both the generation time and the time between mutations are exponentially distributed (see Materials and methods).

Size of clusters of identical sequences

We defined clusters of identical sequences as subsets of epidemiological clusters, which are defined as groups of infections with a known epidemiological link (9). Whereas epidemiological clusters end when every transmission chain composing them ceases to circulate (*i.e.* does not produce any offspring), we define clusters of identical sequences as ending when each transmission chain dies out or results in a mutation event (Figure 1C). Figure 1D depicts how the distribution of the size of clusters of identical sequences was impacted by assumptions regarding the transmission parameter R and k. For example, higher values of R would result in larger clusters of identical sequences. For a fixed R, lower values of k (corresponding to a higher heterogeneity in transmission) would result in a lower probability for a cluster size to reach a certain size. This suggests that the size distribution of clusters of identical sequences might be used to estimate outbreak transmission parameters. Assumptions regarding the reproduction number, the dispersion parameter, and the probability that transmission occurs before mutation also impacted the extinction probability of a cluster of identical sequences and the time to cluster extinction (Figure S1).

Contribution of superspreading events to the size of polytomies

A higher degree of transmission heterogeneity is associated with a higher probability for large transmission events to occur (5) and hence larger clusters of identical pathogen sequences. These large clusters will however not stem solely from a single superspreading event but also from transmission chains prior or after this large transmission event. In Figure 1E-F, we explored to what extent the largest transmission event within a cluster was contributing to the size of the cluster. We found that larger clusters of identical sequences corresponded to larger superspreading events (Figure 1E). As transmission heterogeneity increased (corresponding to lower values of k), the largest transmission event tended to contribute to a higher fraction of the overall cluster size (Figure 1E-F). For example, assuming a reproduction number R of 1 and a probability p that transmission occurs before mutation of 0.7, the median contribution of the largest transmission event to clusters of identical sequences greater than 140 was 13%, 17% and 21% for values of k of 1.0, 0.1 and 0.05 respectively.

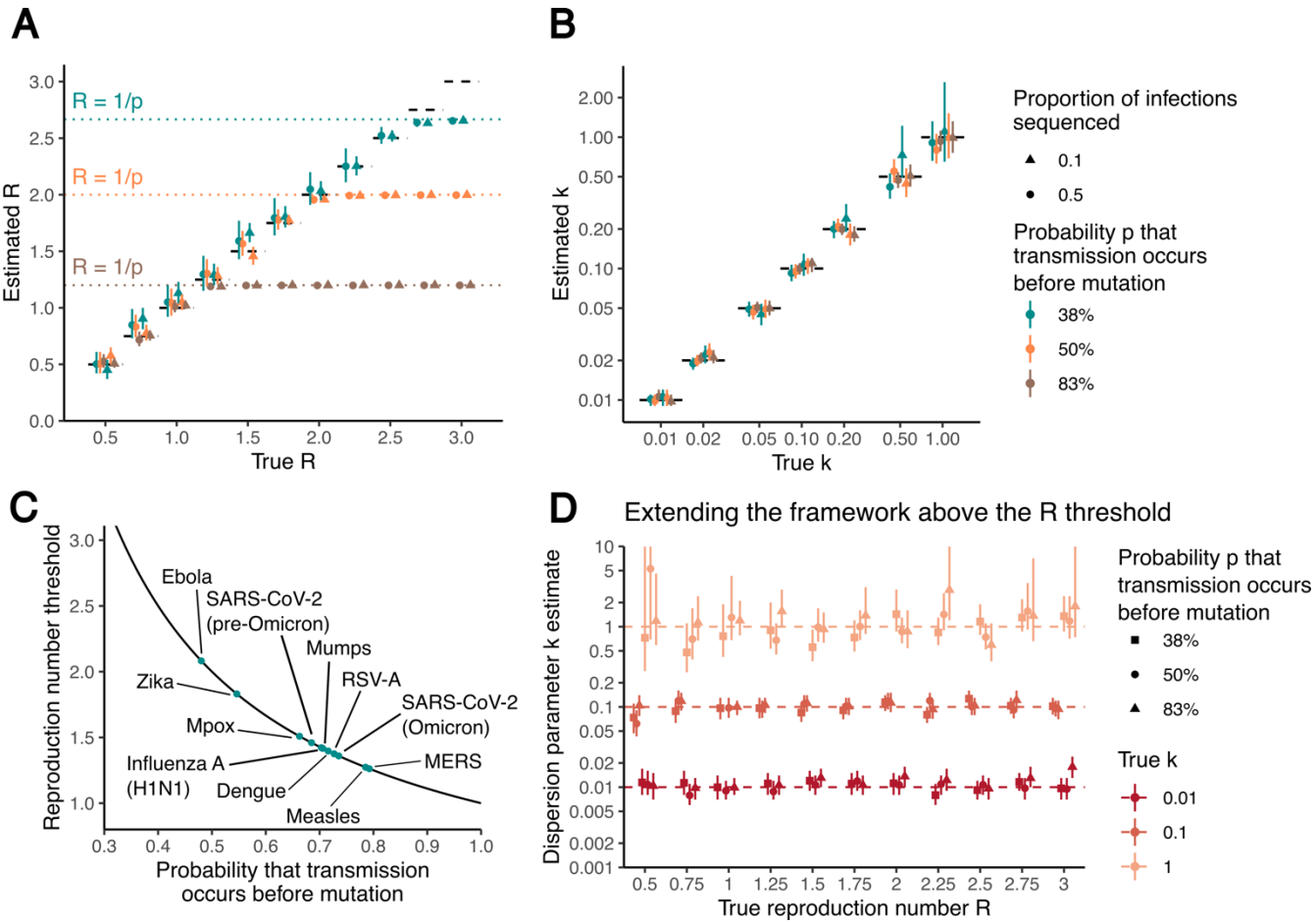

Figure 2: Inference of the reproduction number and the dispersion parameter from synthetic clusters of identical pathogen sequences. A. Estimates of the reproduction number R as a function of the true parameter value used to simulate synthetic clusters. **B.** Estimates of the dispersion parameter k as a function of the true parameter value used to simulate synthetic clusters. **C.** Relationship between the reproduction number threshold and the probability that transmission occurs before mutation (black line) along estimates (points) for a range of pathogens. **D.** Estimates of the dispersion parameter k when conditioning the inference on cluster extinction as a function of the true reproduction number R used to generate synthetic clusters. In A,B,D, point estimates correspond to maximum-likelihood estimates and vertical segments to 95% likelihood profile confidence interval obtained from analyzing 1000 synthetic clusters of identical sequences. Results in A correspond to the joint inference of R and k for true values of k equal to 0.1. Results in B correspond to the joint inference of R and k for true values of R equal to 1.0. Different proportions of sequencing among infections are explored (10% and 50%). In A,B,D, different probabilities p of transmission occurring before mutation are explored.

Inference of transmission parameters from the size distribution clusters of identical sequences

Next, we developed a likelihood-based statistical framework to infer the transmission parameters R and k from pathogen sequence data, based on a value of p (the probability that transmission occurs before mutation) and considering that solely a certain fraction of infections would be sequenced. We evaluated our inference framework on simulated data generated under different assumptions regarding the reproduction number, the dispersion parameter, the probability that transmission occurs before mutation and the fraction of infections sequenced. Figure 2A depicts the relationship between estimates of the

reproduction number R and the true value used to generate synthetic clusters. We were able to correctly recover estimates of the reproduction number at lower values. However, when the reproduction number reached a given threshold, we became unable to accurately estimate its value, with our estimates remaining *stuck* at the threshold value. Interestingly, the threshold values were equal to the inverse of the probability that transmission occurs before mutation, with hence higher threshold values being associated with lower probabilities for transmission to occur before mutation. Below the reproduction number threshold of $1/p$, increasing the number of clusters included in our analysis improved the precision of our estimates (Figure S2). When R remained below the reproduction number threshold, we were able to correctly infer the value of the dispersion parameter k (Figure 2B, Figure S3). Relying on a low number of clusters for the inference resulted in overestimates of the dispersion parameter (Figure S3) and underestimates of the reproduction number, in line with previous studies on the ability to infer parameters from a negative binomial distribution (9,19). For values of R higher than the threshold, we were unable to correctly infer the dispersion parameter, with values consistently overestimated and a bias that increased with both k and the expected mean number of offspring of identical sequences (Figure S4, Figure S5).

Reproduction number threshold for different acute infections

The R threshold value below which our inference framework will produce unbiased estimates will thus depend both on the natural history of the infection and the evolutionary characteristics of the pathogen. We explored how this threshold varied for a range of viruses (Figure 2C, Table S1). For Severe Acute Respiratory Syndrome (SARS), we estimated a probability for transmission to occur before mutation of 9%, thus resulting in a R threshold value higher than 10. This observation is consistent with previous work highlighting the value of genome sequences in reconstructing SARS-CoV-like outbreaks (11). For the other pathogens we considered, values of the probability that transmission occurs before mutation li situations where the probability of cluster extinction ed between 48% (for Ebola) and 79% (for Middle Eastern Respiratory Syndrome (MERS)), corresponding to R thresholds between 1.26 and 2.08.

Inference of transmission parameters conditional on cluster extinction

Our first method provides reliable estimates of both R and k when the mean number of offspring with identical sequences is lower than 1 ($R \cdot p < 1$), corresponding to situations where cluster extinction is certain. Our method however becomes unreliable when the probability of cluster extinction is strictly lower than 1. We previously relied on the full distribution of clusters of identical sequences, including those that did not go extinct (which were then set to an arbitrary high threshold value). An alternative approach would consist in looking at cluster sizes conditional on extinction (20,21). Previous theoretical work has indeed shown that a supercritical epidemic process where extinction is uncertain (characterized by R > 1) can be mapped to a subcritical counterpart characterized by a mean number of offspring lower than 1 (R < 1) and the same dispersion parameter (20). We hence adapted this framework to look at the size of clusters of identical sequences (see Methods) conditional on them having gone extinct. Using this statistical framework, we were able to infer values of the dispersion parameter even when the mean number of offspring with identical sequences was greater than 1 (Figure 2D, Figure S6). This framework enables estimating the reproduction number for clusters that have gone extinct (Figure S7). Assuming prior knowledge on whether the reproduction number lies above or below the threshold of 1/p, the estimated subcritical reproduction number can either directly be interpreted as the reproduction number of the outbreak (below the threshold) or mapped to a corresponding reproduction number higher than 1/p (Figure S8).

Overall, our inference framework provided unbiased estimates of both R and k when the mean expected number of offspring with identical genomes lies below 1. When reaching this critical threshold, estimates of the reproduction number became biased downwards. In this parameter regime, estimates of the

dispersion parameter may also be biased and could be interpreted as an upper bound. We then introduced an alternative approach to infer k in this parameter regime. In the following, we focus on situations where the reproduction number lies below the critical threshold of $1/p$ and we report a series of analyses showcasing how our method may be applied in different epidemiological settings.

Recovering characteristics of the Middle East Respiratory Syndrome (MERS) outbreak (2013-2015)

MERS is a respiratory infection first identified in 2012, associated with a case fatality ratio of around 40%. MERS is transmitted to humans either upon contact with infected camels, who act as a zoonotic reservoir, or with infected humans (22). Human-to-human transmission however results in subcritical transmission chains (R < 1) (23–27) characterized by substantial heterogeneity (25,26). We analysed 174 MERS-CoV human sequences sampled between 2013 and 2015 (27) and identified 140 clusters of identical sequences, with an average cluster size of 1.2 (Figure 3A). Assuming all infections were detected, we estimated a reproduction number of 0.57 (95% confidence interval (CI): 0.45-0.70) and a dispersion parameter of 0.14 (95% CI: 0.04-0.47) (Figure 3B-C, Table S2). These estimates were consistent with those obtained from the analysis of the size of MERS epidemiological clusters (25). Interestingly, our confidence intervals were narrower than the ones obtained from the analysis of epidemiological clusters.

Epidemiological surveillance is generally able to only detect a fraction of the overall infection burden, and skewed towards symptomatic or severe outcomes. For MERS, modelling studies have suggested that detected cases may have accounted for only around half of overall infections (28). In this scenario, we estimated a higher value of 0.64 (95%CI: 0.53-0.76) for the reproduction number and a lower value of 0.09 (95%CI: 0.03-0.26) for the dispersion parameter k (corresponding to a higher degree of heterogeneity in transmission) (Figure 3B-C, Table S2). Estimates were however qualitatively similar to the ones obtained assuming infections were completely detected.

Characterizing measles transmission in the post-vaccination era

During the last decade, European countries have experienced important measles outbreaks despite elevated vaccination coverages. Such outbreaks may occur either due to insufficient population vaccination coverage or due to persisting pockets of low vaccination rates (29,30). Here, we estimate transmission parameters during the 2017 measles outbreak that occurred in the Veneto Region in Italy from 30 sequences sampled during this time period (31) (Figure 3D). Assuming all infections were detected, we estimated a reproduction number R of 0.57 (95%CI: 0.29–1.15) and a dispersion parameter k of 0.04 (95%CI: 0.003-0.45) (Figure 3E-F, Table S3). We also conducted a sensitivity analysis assuming that 50% of infections may have gone undetected. We obtained an estimate of R of 0.61 (95%CI: 0.32-1.15) and of k of 0.02 (95%CI: 0.002-0.19) (Figure 3E-F, Table S3). Our estimates of the reproduction number were similar to those obtained for measles outbreaks occurring in high-income countries in the post-vaccination era (10,32). Due to the limited number of clusters of identical sequences included in our analysis, the uncertainty around our estimate of the dispersion parameters remains quite substantial. Our results yet suggest a high degree of heterogeneity, in line with previous analyses (5,10).

Severe acute respiratory syndrome coronavirus 2 (SARS-CoV-2) transmission heterogeneity during a Zero-COVID strategy

We next focused on the characteristics of the coronavirus disease 19 (COVID-19) epidemic in New Zealand between April 2020 and July 2021, a period during which the epidemic was mostly suppressed without reported community transmission. We applied our modelling framework to SARS-CoV-2 sequences collected during this timeframe. We split the study period into 4 subperiods: April-May 2020, June-December 2020, January-April 2021 and May-July 2021 (Figure 3G) during which respectively 25%, 51%, 46% and 48% of cases were sequenced. We allowed the reproduction number to vary

between periods but assumed that transmission heterogeneity remained constant throughout. Assuming that 80% of infections were detected, we estimated reproduction numbers below unity throughout the period (Figure 3H, Table S4) and a dispersion parameter k of 0.63 (95%CI: 0.33-1.56) (Figure 3I, Table S4), which corresponds to 23-25% (17-30%) of individuals being responsible for 80% of infections throughout the period. We explored the impact of our assumption regarding the fraction of infections detected on our estimates and found that values ranging between 50 and 100% would not quantitatively change our findings (Figure 3H-I, Table S4). Our results are consistent with previous SARS-CoV-2 overdispersion estimates (33).

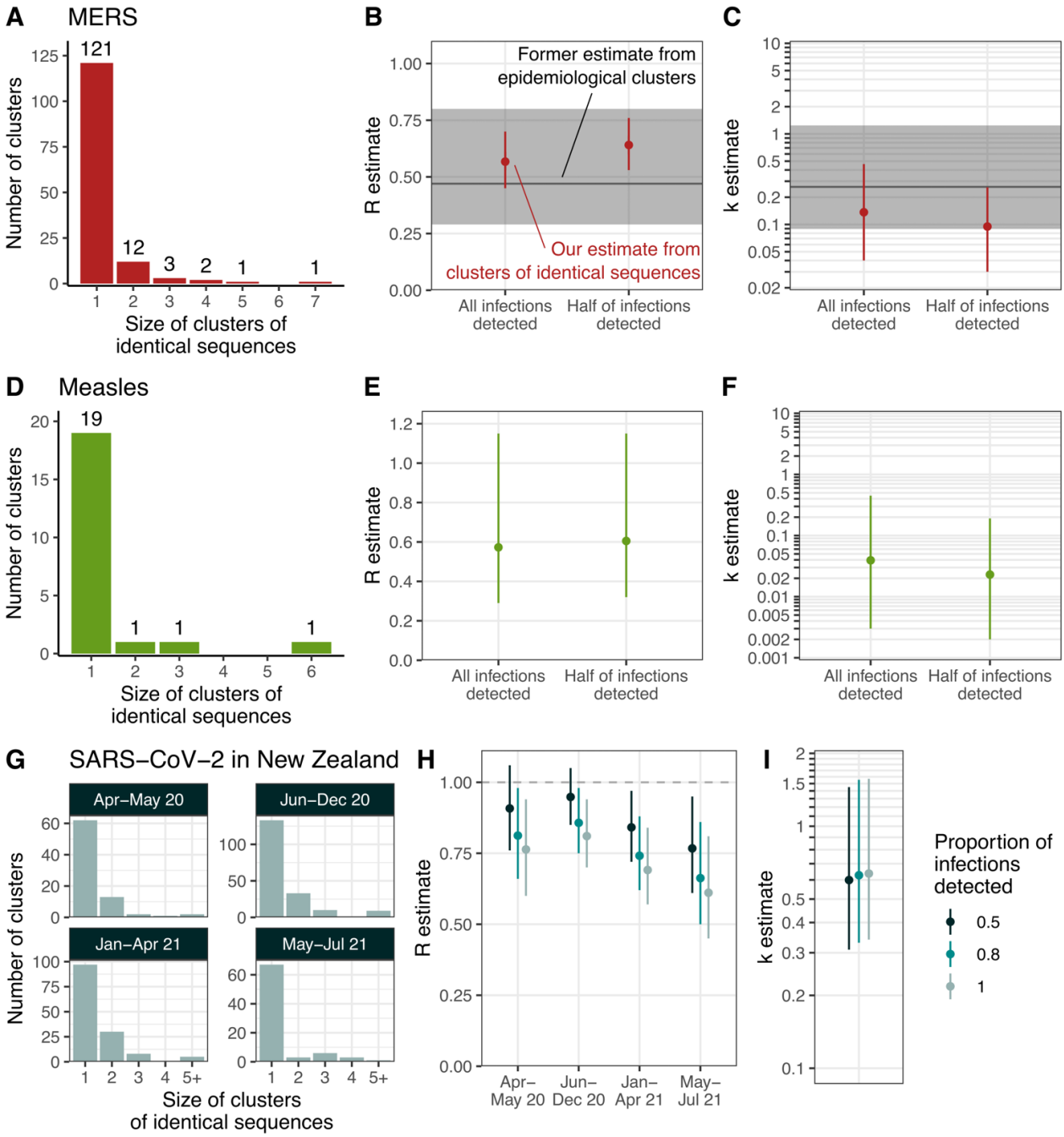

Figure 3: Application of our modelling framework to different pathogen genome datasets. A. Distribution of the size of clusters of identical sequences during the 2013-2015 MERS outbreak (27).

Estimates for MERS of **B.** the reproduction number R and **C.** the dispersion parameter k assuming that all or half of infections were detected. **D.** Distribution of the size of clusters of identical sequences during the measles 2017 outbreak in the Veneto region in Italy (31). Estimates for measles of **E.** the reproduction number R and of **F.** the dispersion parameter k assuming that all or half of infections were detected. **G.** Distribution of the size of clusters of identical sequences during the COVID-19 pandemic in New Zealand by period. Estimates of **H.** the reproduction number R and **I.** the dispersion parameter k for SARS-CoV-2 in New Zealand. For B, C, E, F, H and I, the points correspond to maximum likelihood estimates and the vertical segments to 95% likelihood profile confidence intervals. In B and C, the horizontal lines (respectively the shaded area) correspond to the maximum-likelihood estimate (respectively the 95% confidence intervals) obtained by Kucharski and Althaus (25) from the analysis of the size of MERS epidemiological clusters.

Monitoring the transmission advantages of genetic variants

In the previous sections, we looked at how we can use the size distribution of polytomies to estimate R and k. We then focused on how the spread of a variant characterized by a transmission advantage can influence the size distribution of clusters of identical sequences. More specifically, we were interested in whether hosts infected with a certain genetic subpopulation significantly infect more individuals than hosts infected with another genetic subpopulation. We aimed to quantify this transmission advantage, which may be impacted by the intrinsic transmissibility of the variant of interest, its ability to escape pre-existing immunity or certain characteristics of the host population (*e.g.* immunity profiles). We developed an inference framework based on statistical hypothesis testing (see Methods) to determine whether some variant and non-variant pathogens are associated with different reproduction numbers from the size distribution of clusters of identical sequences observed in these two genetic populations (Figure 4A). In the following, we will refer to variant as the more transmissible genetic subpopulation. However, the role of the variant and the non-variant are interchangeable, making our results hence directly applicable for a less transmissible one.

We evaluated the ability of our statistical framework to detect the presence of a transmission advantage given the number of genetic clusters observed and the magnitude of this transmission advantage (Figure 4B). We found that (i) the sensitivity of our test increased when more clusters of identical sequences were observed and that (ii) the detection of small transmission advantages required the analysis of a larger number of clusters. When the reproduction number of the variant reached the threshold of $1/p$, the sensitivity of our test decreased. We showed that our inference framework provided unbiased estimates of the transmission advantage and that the overall precision increased as a larger number of clusters of identical sequences were analyzed (Figure 4C) as long as both the reproduction number of the variant and the non-variant remained below the $1/p$ threshold (Figure S9). Interestingly, sensitivity remained high even above the threshold when a sufficiently large number of clusters were included in the analysis. We also found that failing to allow for the reproduction number to differ between two genetic subpopulations resulted in overestimating the extent of transmission heterogeneity (Figure 4D, Figure S10).

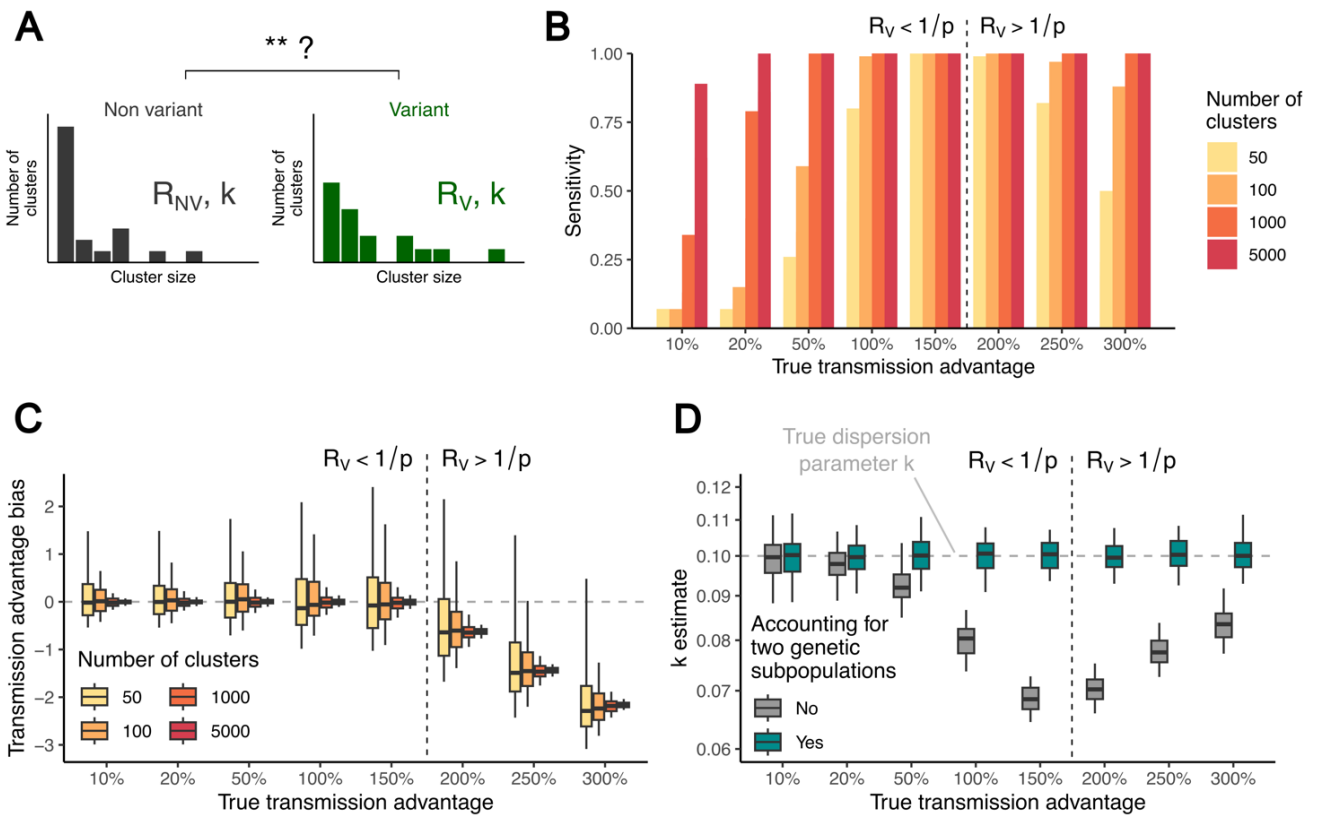

Figure 4: Performance of our inference framework in quantifying the transmission advantage of genetic variants from the size distribution of polytomies. A. We aim to compare the size distribution of clusters of identical sequences splitting a given pathogen between variant and non-variant subtypes. **B.** Sensitivity of the analysis of clusters of identical pathogen sequences in detecting a change in the transmissibility of a genetic variant. This is done for different values of the true transmission advantage and exploring different sizes of datasets on which the inference is based. **C.** Transmission advantage bias for different values of the true transmission advantage and exploring different sizes of datasets on which the inference is based. **D.** Impact of accounting for two genetic subpopulations on estimates of the dispersion parameter. The transmission advantage bias is defined as $\frac{R_V^{MLE}}{R_{NV}^{MLE}} - \frac{R_V^{true}}{R_{NV}^{true}}$ where R_V^{MLE} (respectively R_{NV}^{MLE}) is the maximum likelihood estimate for the reproduction number of the variant (respectively the non-variant) and R_V^{true} (respectively R_{NV}^{true}) is the true reproduction number of the variant (respectively the non-variant) used to generate synthetic cluster data. In B-D, the vertical dashed line delimits the regions where the reproduction number of the variant is above/below the threshold of 1/p. In B-D, the results correspond to scenarios where the true dispersion parameter is equal to 0.1, the probability that transmission occurs before mutation to 0.5 and the reproduction number of the non-variant to 0.75. In D, the results correspond to analyses based on 5,000 clusters of identical sequences for both the variant and the non-variant.

Application to SARS-CoV-2 variants in Washington state

To illustrate our framework, we analysed SARS-CoV-2 sequence data collected in Washington state, in the United States (Figure 5A, Figure S11). Figure 5B depicts the mean size of clusters of identical sequences for different variants depending on the month of first detection of the cluster in Washington

state. We found that the dynamics of the mean size of clusters of identical sequences reflected the dynamics of strain replacement in Washington state (Figure 5A), with greater average cluster sizes being observed when a given variant of concern was increasing in proportion. This pattern is expected as we showed that average cluster sizes can be related to the effective reproduction number. Other elements (such as the fraction of infections sequenced) are susceptible to impact patterns of cluster sizes.

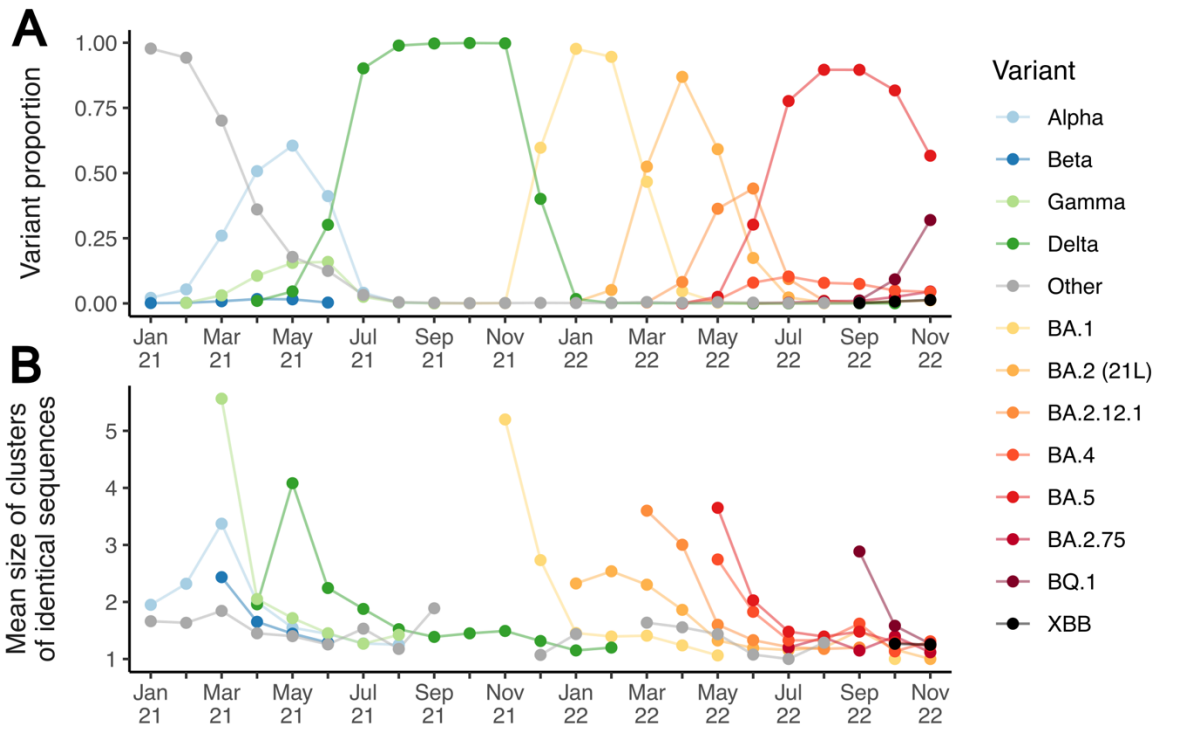

C

	10%	20%	50%	80%
Omicron (BA.4, BA.5)	$1{\cdot}10^{-5}$	$1{\cdot}10^{-5}$	$1{\cdot}10^{-5}$	$1{\cdot}10^{-5}$
Omicron (BA.2)	$< 1{\cdot}10^{-5}$	$< 1{\cdot}10^{-5}$	$< 1{\cdot}10^{-5}$	$< 1{\cdot}10^{-5}$
Omicron (BA.1)	$< 1{\cdot}10^{-5}$	$< 1{\cdot}10^{-5}$	$< 1{\cdot}10^{-5}$	$< 1{\cdot}10^{-5}$
Delta	$7{\cdot}10^{-5}$	$8{\cdot}10^{-5}$	$9{\cdot}10^{-5}$	$9{\cdot}10^{-5}$
Alpha	$< 1{\cdot}10^{-5}$	$< 1{\cdot}10^{-5}$	$< 1{\cdot}10^{-5}$	$< 1{\cdot}10^{-5}$
Epsilon	$3.5{\cdot}10^{-2}$	$3.5{\cdot}10^{-2}$	$3.5{\cdot}10^{-2}$	$3.5{\cdot}10^{-2}$
D614G	$4.1{\cdot}10^{-1}$	$4.1{\cdot}10^{-1}$	$4.2{\cdot}10^{-1}$	$4.2{\cdot}10^{-1}$

Proportion of infections detected

Significance level
< 1%
< 5%
Non significant at 5%

Figure 5: Analysis of SARS-CoV-2 clusters of identical sequences in Washington state. A. Proportion of variant among sequences by month of sample collection. **B.** Mean size of clusters of identical sequences in Washington state from 2021 across different SARS-CoV-2 clades. **C.** P-values associated with different SARS-CoV-2 variants for the COVID-19 pandemic in Washington state for different assumptions regarding the fraction of infections detected. In B, we report the mean size of clusters of identical sequences grouping clusters depending on their first detection date. In B, we display

the mean cluster size for a given month and a given variant if at least five clusters of identical sequences were detected (for this variant this month). The variants dynamics were derived based on Nextstrain clades allocation (34,35).

In the early stages of their spread, variants of concerns (VOCs) such as Alpha, Delta or Omicron have been associated with initially short doubling times (36–39), corresponding to reproduction numbers above the threshold of $1/p$. This, alongside other factors such as changes in the reproduction number over time or the implementation of stringent control measures to slow the epidemic spread, could result in biased estimates of the transmission advantage. To overcome this caveat and avoid overinterpreting our results, we instead focused on whether we were able to detect a transmission change as we previously saw that sensitivity remained high for large cluster datasets. We tested a list of variants on whether they were associated with a transmission advantage (or disadvantage) compared to the other strains that were circulating during this time period. The p-values for different variants and different assumptions regarding the proportion of infections detected are depicted in Figure 4F. We note that lower p-values should not be interpreted as corresponding to higher transmission advantages but rather indicate stronger statistical support for a difference in transmissibility. We did not find evidence for the D614G mutation, that occurred early on during the pandemic, to be associated with an increased transmissibility, which has been suggested by other studies (40,41). For Alpha, Delta, and Omicron (BA.1, BA.2 and BA.4/BA.5), we found statistical support for them to be associated with a different transmission level compared to other lineages that circulated at that time. For the VOC Epsilon, we found a p-value of around 2% suggesting that it might be associated with a different transmission intensity.

Discussion

The extent of heterogeneity in transmission and the transmissibility of a pathogen have important implications regarding both its potential epidemic burden and the impact of control measures. Despite their epidemiological relevance, estimating these two parameters has remained delicate during most outbreaks. In this work, we presented a novel modelling framework enabling the joint inference of the reproduction number R and the dispersion parameter k from the size distribution of clusters of identical sequences. We evaluated the performance of our statistical framework and subsequently applied it to a range of epidemiological situations. Finally, we showed how it may be extended to look at the relative transmissibility of different genetic subpopulations.

Robust estimates of key epidemiological parameters (such as the reproduction number R and the dispersion parameter k) are critical to ascertain epidemic risks. They can be obtained by directly analyzing chains of transmission (5) , though such data are generally delicate or almost impossible to collect for some pathogens (42). Establishing epidemiological links between cases may indeed be hampered by widespread community transmission, sub-clinical disease manifestation or when the infection is spread through a vector. Alternatively, it has been shown that the size distribution of epidemiological clusters can be harnessed to obtain such estimates (9,43). Beyond the potential challenges in establishing epidemiological links between cases, apparent epidemiological clusters may involve different transmission chains, that couldn't be disentangled without further molecular investigation. This is for example the case in the measles outbreak reported in Pacenti et al. (31), that we analysed here, where one observed epidemiological cluster was actually constituted of two evolutionary groups. Relying on the size of epidemiological clusters would thus likely lead to overestimating the reproduction number. Here, we proposed a new approach, exploiting the relationship between epidemiological clusters and clusters of identical sequences to provide robust estimates of both R and k which does not require to reconstruct these epidemiological relationships. Interestingly, we obtained narrower confidence intervals for MERS

transmission parameters than the ones obtained from the analysis of the size of epidemiological clusters (25). This can likely be explained by the greater number of clusters (though smaller) included in our analysis. This suggests that even in settings where transmission chains may be reconstructed, the combination of case investigation with pathogen sequencing may be valuable to increase statistical power and our ability to estimate these key epidemiological parameters. Moreover, as estimates may be biased upwards for the dispersion parameter and downwards for the reproduction number when relying on a low number of clusters for the analysis (Figure S2) (9,19), the inclusion of a larger number of clusters enabled by looking at genetic clusters instead of epidemiological ones can reduce biases.

High-throughput sequencing has enabled the faster and cheaper generation of pathogen genome sequences. Current tree-based methods nonetheless require heavy computations to estimate growth rates from pathogen genomes. Here, we showed that the size of clusters of identical sequences directly contains an imprint of the underlying epidemiological processes and can be leveraged to characterize the intensity and heterogeneity in transmission, this without requiring the estimation of the associated phylogenetic tree. Moreover, the speed and ease of implementation of our method could make it valuable for public health professionals who may not have access to or be comfortable using scientific software programs currently used for phylodynamic analysis. The concept of phylodynamics has been introduced to describe how epidemiological, immunological and evolutionary processes shape pathogen phylogenies (14,15). Here, we hence introduced in essence a new phylodynamic framework describing how the size of polytomies is influenced by epidemic dynamics. Importantly, our approach could help to interpret sequence data in the early stage of an outbreak when genetic diversity is still limited (e.g. below the phylodynamic threshold) (44) and phylogenetic uncertainty is high. This may though require adapting our method to account for right-truncated clusters of identical sequences.

Detecting changes in the reproduction number and in the transmissibility of genetic variants is a crucial element of epidemic preparedness. Former modelling efforts have underlined the value of monitoring anomalous epidemiological cluster size for epidemic surveillance (9,43). Here, we developed an analogous framework to determine whether a genetic variant was characterized by a different reproduction number. This was done by comparing the size distribution of clusters of identical sequences between two pathogen genetic populations. Interestingly, a simple visual inspection of these distributions for the Alpha, Delta and Omicron variants of concerns (VOCs) in Washington state was already suggesting that VOCs were associated with larger polytomy sizes (Figure S11). This means that it should be possible to set up a surveillance system monitoring the size of clusters of identical sequences to detect anomalous chains, which may be attributable to changes in the reproduction number or increased transmissibility of genetic variants.

Our modelling framework relies on the assumption that two identical sequences are always linked within an epidemiological cluster. This hypothesis could be broken if an identical sequence was introduced multiple times in a given population. To account for such repeated introductions, our likelihood calculation could easily be extended to integrate over the potential sub-clusters of identical sequences by adapting the combinatorial approach proposed by Blumberg and Lloyd-Smith (9). We also assumed that no convergent evolution was occurring. We also assumed that the probability for an infected individual to be sequenced did not depend on its infectivity profile. If sequencing was biased towards individuals with lower cycle threshold (Ct) values, the sequence dataset might over-represent individuals who are more infectious, which could impact estimates. Finally, our inference results were based on some assumptions on the probability p that a pathogen sequenced in a secondary case has the same genome than a pathogen sequenced in its infector. Here, we reduced this probability to the probability that a transmission event occurs before a mutation one, which should hold for most infectious diseases causing acute infections with limited within-host diversity and relatively short generation times.

Our work opens up a number of exciting research directions, such as accounting for reproduction numbers varying over time (2), considering more complex observation processes (10), evaluating how heterogeneity in infectious duration is susceptible to impact transmission heterogeneity estimates (45), or extending our approach to pathogens responsible for longer infections characterized by considerable within-host diversity (*e.g.* by assessing how the reproduction number and the dispersion parameter may impact the pathogen genetic diversity at the population level (46)). We also showed that when the reproduction number reaches the threshold of $1/p$, where p is the probability that transmission occurs before mutation, our approach is no longer valid as it leads to biased estimates of the reproduction number and of the dispersion parameter. Compared with previous methods relying on the size of epidemiological clusters, we extended the threshold by looking at genomic clusters as these initial methods can just be considered as a special case of our method with $p = 1$. We also suggested an alternative method to estimate the dispersion parameter when reaching this threshold by only considering clusters that got extinct. However, we acknowledge that determining in practice whether a cluster of identical sequences has become extinct may be challenging. Overall, future research extending our framework to values of R lying above the threshold (*e.g.* by also including the sequence collection date) would be of primary interest.

Building on the observation that clusters of identical sequences are nested within epidemiological clusters, we introduced a novel statistical framework to (i) infer the reproduction number and transmission heterogeneity from pathogen genomes and (ii) determine whether a specific variant subpopulation is characterized by a transmission advantage. Our method is suitable to analyse epidemics even when establishing epidemiological relationships is difficult (*e.g.* vector-borne infections), which was the foundation of previous methods used to quantify transmission heterogeneity, hence constituting a valuable new tool to study current epidemics and prepare for future ones.

Material and methods

Offspring with identical genomes distribution

We used a branching process formulation to derive the distribution of the number of offspring with identical genomes. Let Z (respectively $\bar{Z}$) be a random variable corresponding to the number of offspring generated by a single infected individual (respectively the number of offspring with identical genomes). Let g and $\bar{g}$ denote their respective probability generating function:

$$\forall\, |s| < 1, \qquad g(s) = \sum_{j \geq 0} P[Z = j] \cdot s^j$$

$$\forall\, |s| < 1, \qquad \bar{g}(s) = \sum_{j \geq 0} P[\bar{Z} = j] \cdot s^j$$

We introduced p as the probability that a transmission event occurs before a mutation event. The distribution of the number of offspring with identical genomes $\bar{Z}$ can then be related to that of the number of offspring stemming from a single infector through a binomial distribution:

$$\bar{Z} \sim B(Z, p)$$

This enabled us to derive the following relationship between g and $\bar{g}$:

$$\forall\, |s| < 1, \qquad \bar{g}(s) = \sum_{j \geq 0} \sum_{j' \geq j} P[\bar{Z} = j \mid Z = j'] \cdot P[Z = j'] \cdot s^j = \sum_{j \geq 0} \sum_{j' \geq j} \binom{j'}{j} \cdot p^j \cdot (1-p)^{j'-j} \cdot P[Z = j'] \cdot s^j$$

$$\forall\, |s| < 1, \qquad \bar{g}(s) = \sum_{j' \geq 0} P[Z = j'] \cdot \sum_{j=0}^{j'} \binom{j'}{j} \cdot (ps)^j \cdot (1-p)^{j'-j} = \sum_{j' \geq 0} P[Z = j'] \cdot (1-p-ps)^{j'}$$

$$\forall\, |s| < 1, \qquad \bar{g}(s) = g(1-p-ps)$$

Following Lloyd-Smith et al.(5), we assumed that the offspring distribution (Z) follows a negative binomial distribution of mean R and dispersion parameter k. The probability generating function g of Z thus had the following form:

$$\forall |s| < 1, \qquad g(s) = \left(1 + \frac{R}{k}(1-s)\right)^{-k}$$

The probability generating function $\bar{g}$ of $\bar{Z}$ could then be derived as:

$$\forall |s| < 1, \qquad \bar{g}(s) = \left(1 + \frac{R \cdot p}{k}(1-s)\right)^{-k}$$

which is the probability generating function of a negative binomial distribution of mean $p \cdot R$ and dispersion parameter k. Hence:

$$\bar{Z} \sim NB(p \cdot R, k)$$

Distribution of the size of clusters of identical sequences

Nishiura et al (8) and Blumberg & Lloyd-Smith (9) developed an inference framework to estimate the reproduction number and the dispersion parameter from the size of epidemiological clusters. Here, we extended this to estimate these two parameters from the size distribution of clusters of identical sequences. Let r_j denote the probability for the size of a cluster of identical sequences to be equal to j. We have:

$$\forall j \geq 1, \qquad r_j = \frac{\Gamma(kj + j - 1)}{\Gamma(kj) \cdot \Gamma(j+1)} \cdot \frac{\left(\frac{pR}{k}\right)^{j-1}}{\left(1 + \frac{pR}{k}\right)^{kj+j-1}} \qquad (1)$$

Accounting for the partial sequencing of infections

In practice, clusters will only be partially observed as (i) solely a fraction of infections may be detected by the surveillance system (we refer to the detected infections as cases) and (ii) solely a fraction of cases will then be sequenced. This means that the observed distribution of the size of clusters of identical sequences will differ from the true underlying size distribution of clusters of identical sequences. Failing to account for this partial observation has been shown to lead to biased estimates of R and k when inferring them from the size distribution of epidemiological clusters (10). Here, we explicitly modeled the cluster observation process.

Let p_{detect} denote the probability that a given infected individual is sequenced. Let s_j denote the probability to observe j identical sequences among an arbitrary cluster of identical sequences for j. We have:

$$\forall j \geq 0, \quad s_j = \sum_{l \geq j} r_l \cdot \binom{l}{j} \cdot (p_{detect})^j \cdot (1 - p_{detect})^{l-j}$$

As clusters of size 0 would never be observed, we were interested in the probability $\tilde{r_j}$ for an observed cluster to be of a given size j knowing in was observed (which corresponds to the probability for an observed cluster to be of size j conditional on this cluster being of size greater or equal to 1):

$$\forall\, j \geq 1, \qquad \tilde{r_j} = \frac{s_j}{1 - s_0}$$

In practice, we approximated s_j with a truncated sum, assuming cluster sizes remained below a certain threshold c_{max}:

$$s_j = \sum_{l=j}^{c_{max}} r_l \cdot \binom{l}{j} \cdot (p_{detect})^j \cdot (1 - p_{detect})^{l-j}$$

Statistical framework

We used a likelihood-based approach to estimate R and k from the size distribution of clusters of identical sequences. Let D denote data describing the size of clusters of identical sequences. Let N denote the number of distinct clusters in D and n_j be the number of clusters of size j. The log-likelihood of the data was derived as:

$$LL(\, R, k \mid D\,) = \sum_{j \geq 1} n_j \ln\left(\tilde{r_j}\right) \qquad (2)$$

Maximum likelihood estimates were obtained using a constrained quasi-Newton optimization approach imposing values of the reproduction number ranging between 0.01 and 10.0 and values of the dispersion parameter ranging between 0.001 and 10.0. This was done using the *optim* base R function (47).

Confidence intervals were obtained by likelihood profiling (9). Let LL^{MLE} denote the maximum log-likelihood of the log-likelihood function of (R, k) defined in (2). We introduced the profile log-likelihood of R as follows:

$$LL_P(R) = \max_k \, LL(R, k)$$

A confidence interval associated with a confidence level of $1 - \alpha$ then corresponds to values of R verifying:

$$2 \cdot \left(LL^{MLE} - LL_P(R)\right) < \chi_1^2(1 - \alpha)$$

where $\chi_1^2(\cdot)$ is the quantile function of a chi-squared distribution with 1 degree of freedom. Confidence intervals for the dispersion parameter k were obtained in a similar manner, by inverting the role of R and k above. The bounds of the confidence intervals were considered unresolved when lying outside the range of 0.01-10 for R and 0.001-10 for k.

Inference from the size of clusters of identical sequences conditional on extinction

We implemented an alternative statistical framework where we this time inferred transmission parameters from the size of extinct clusters of identical sequences. If the mean number of offspring with identical sequences (equal to $R \cdot p$) is lower than 1, the probability of cluster extinction is equal to 1 and this statistical framework is equivalent to the one presented above. If the mean number of offspring with identical sequences is higher than 1, the probability ϵ of cluster extinction is lower than 1 and the results will differ. We extended the formalism introduced by Waxman and Nouvellet (20) who showed that,

conditional on extinction, supercritical and subcritical dynamics (respectively characterized by a reproduction number below and above 1) cannot be distinguished. The main difference lies in that we here do not consider finite disease outbreaks but finite *mutation-less* outbreaks, *i.e.* clusters of infected individuals characterized by the same pathogen sequence.

The probability for a cluster of identical sequences to be of size j knowing it got extinct is equal to (20,21):

$$r_j^{extinct} = \frac{\Gamma(kj+j-1)}{\Gamma(kj)\cdot\Gamma(j+1)} \cdot \frac{\left(\frac{pR_s}{k}\right)^{j-1}}{\left(1+\frac{pR_s}{k}\right)^{kj+j-1}} \cdot \epsilon$$

where $R_s = R \cdot \epsilon^{1+1/k}$ is the reproduction number associated with clusters of identical sequences that got extinct. We thus have $R_s < 1/p$. In the specific situation where $R < 1/p$, we have $\epsilon = 1$ and $R = R_s$ so that $r_j^{extinct} = r_j$.

We hence extended the inference framework developed in the former section to cluster size conditional on extinction by replacing r_j by $r_j^{extinct}$ and R by R_s in all equations. Maximum likelihood estimates of R_s and k were then obtained by imposing values of the reproduction number ranging between 0.01 and $1/p$ and values of the dispersion parameter ranging between 0.001 and 10.0.

Probability that transmission occurs before mutation for an exponentially distributed generation time

Let μ denote the virus mutation rate (per day). Assuming a Poisson process for the occurrence of mutations, the waiting time before the occurrence of a mutation (T_{mut}) follows an exponential distribution of rate μ and mean $d_{mut} = 1/\mu$. If the generation time (T_{gen}) follows an exponential distribution of rate $1/d_{gen}$, assuming that T_{gen} and T_{mut} are independent, the probability p that a transmission event occurs before a mutation one is equal to:

$$p = P\left[T_{gen} < T_{mut}\right] = \int_{t_{gen}=0}^{+\infty} \int_{t_{mut}=t_{gen}}^{+\infty} \frac{1}{d_{mut}} \cdot \frac{1}{d_{gen}} \cdot e^{-\frac{t_{gen}}{d_{gen}}} \cdot e^{-\frac{t_{mut}}{d_{mut}}} \cdot dt_{gen} \cdot dt_{mut}$$

$$p = \frac{d_{mut}/d_{gen}}{d_{mut}/d_{gen}+1}$$

Simulation approach to estimate the probability that transmission occurs before mutation using a more flexible framework for the generation time

The generation time can often not be approximated using an exponential distribution (e.g. its variance is generally not equal to its mean). We relaxed this assumption and empirically derived the probability that a transmission event occurs before a mutation one using a simulation approach for the following pathogens: DENV-1 (dengue virus 1), mumps virus, MERS-CoV, SARS-CoV, Ebola virus, Mpox during the 2022-2023 outbreak, measles virus, RSV, Zika virus, Influenza A (H1N1pdm) and SARS-CoV-2. For SARS-CoV-2, we accounted for a reduction in the generation time for Omicron variant (48,49). For each pathogen, we identified relevant parameters describing the mean and the standard deviation of the generation time of these pathogens. As a reminder, the generation time describes the average duration between the infection time of an index case and the time at which this primary case infects a secondary case. We then drew $n_{sim} = 10^7$ generation intervals from a Gamma distribution parametrized with the same mean and standard deviation. We also drew $n_{sim} = 10^7$ delays until the occurrence of a first mutation for these different pathogens from an exponential distribution of rate the mutation rate obtained from the literature. We then computed the proportion of simulations for which the generation time was shorter than

the delay until the occurrence of a first mutation to obtain an estimate of the probability that transmission occurs before mutation. Parameters used in the simulations along the resulting probability estimate are detailed in Table S1. A visual comparison of the distribution of the delay before a mutation and a transmission event is available in Figure S12.

Simulation study

We used a simulation study to evaluate our two inference frameworks (unconditional and conditional on cluster extinction). We simulated a branching process with mutation assuming:

- different values for the probability that transmission occurs before mutation (38%, 50% and 83% which correspond to values of the ratio d_{mut}/d_{gen} defined above of 0.6, 1 and 5 respectively).
- different values for the proportion of infections sequenced p_{detect} (50% and 10%)
- different values of the reproduction number R (ranging between 0.5 and 3.0)
- different values for the dispersion parameter k (ranging between 0.01 and 1.0)

For each parameter combination, we explored the performance of our statistical framework on a dataset comprised of 50, 100, 1000 or 5000 clusters of identical sequences. Clusters of identical sequences were generated using a branching process. As some clusters may never get extinct, clusters were simulated until reaching a size of 10,000. For the first inference framework (unconditional on extinction), we used the full simulated cluster dataset (including those that reached 10,000). For the second inference framework (conditional on extinction), we considered that clusters that reached 10,000 did not go extinct and removed them from the cluster dataset. We then accounted for the partial sequencing of infections by drawing the observed cluster sizes from a binomial distribution with probability parameter p_{detect}.

Inference framework to quantifying the transmission advantage of genetic variants

We next extended our inference framework to study the transmission advantage of a specific genetic variant. This was done by performing a likelihood ratio test to determine whether the size distribution of clusters of identical pathogen sequences for a specific variant (superscript V) corresponds to a different reproduction number than the size distribution of clusters of identical pathogen sequences for non-variant sequences (superscript NV). Similar methods have been used to monitor changes in the reproduction number from epidemiological cluster data (9). We assumed that the variant and the non-variant pathogen had the same dispersion parameter k.

More specifically, let D^V (respectively D^{NV}) denote the data describing the size of cluster of identical sequences for the variant (respectively the non-variant). We first computed the log-likelihood of the combined dataset $D_{combined} = (D^V, D^{NV})$ assuming that the variant and the non-variant were both characterized by the reproduction number R and the dispersion parameter k: $LL_{combined}(R, k \mid D_{combined})$. We then estimated the maximum-likelihood estimates of this combined likelihood $(R^{MLE}_{combined}, k^{MLE}_{combined})$. We then computed a second splited log-likelihood, this time assuming that the variant and the non-variant qere respectively characterized by the reproduction numbers R^V and R^{NV}:

$$LL_{split}(R^V, R^{NV}, k \mid D^V, D^{NV}) = LL(R^V, k \mid D^V) + LL(R^{NV}, k \mid D^{NV})$$

We then computed the corresponding maximum likelihood estimates $(R^{V,MLE}, R^{NV,MLE}, k^{MLE}_{split})$. As $LL_{combined}$ is nested within LL_{split}, we performed a likelihood ratio test by computing the following test statistic:

$$\lambda_{LRT} = -2 \cdot \left[LL_{combined}\left(R^{MLE}_{combined}, k^{MLE}_{combined} \mid D_{combined}\right) - LL_{split}\left(R^{V,MLE}, R^{NV,MLE}, k^{MLE}_{split} \mid D^V, D^{NV}\right) \right]$$

We then derived the corresponding p-value under a chi-squared distribution with 1 degree of freedom. In all the analyses reported in the manuscript, we used a type I error (Alpha risk) of 5%.

Simulation study to evaluate the performance of our inference framework

We used a simulation study to ascertain the performance of our inference framework. Synthetic cluster data were generated from a branching process and exploring a range of assumptions regarding:

- the variant transmission advantage (defined as $\frac{R^V}{R^{NV}} - 1$)
- the probability that transmission occurs before mutation
- the dispersion parameter
- the reproduction number of the non-variant
- the number of clusters simulated for both the variant and the non-variant (50, 100, 1000, 5000)

For each combination of parameters, we evaluated the sensitivity of our statistical framework in detecting a difference between the reproduction numbers of two genetic subpopulations. This was done running our inference framework on 100 different datasets generated using the same set of parameters. For each combination of parameters, we then computed the sensitivity as the fraction of simulations for which we were able to detect a transmission advantage using a significance level of 5%. We also computed the absolute transmission advantage bias as the difference between the estimated transmission advantage (maximum-likelihood estimate) and the true one.

Application to different epidemiological situations

2013-2015 Middle East respiratory syndrome outbreak

Between March 2012 and 31 December 2015, 1,646 cases were identified globally (50). We analysed 174 aligned MERS-CoV sequence data sampled in humans between 2013 and 2016 analysed in Dudas et al (27) and made available at (51). This set of sequences thus corresponded to 10.6% of all detected cases. For the analysis, we explore scenarios where:

(i) all infections where ddetected (corresponding to an infection sequencing ratio of 10.6%)
(ii) half of infections where detected (corresponding to an infection sequencing ratio of 5.3%)

For the MERS analysis, we used a threshold c_{max}.for the size of cluster of 10,000. Increasing this value to 50,000 did not impact our estimates.

2017-2018 measles outbreak in the Veneto Region (Italy)

We used data describing the 2017-2018 measles outbreak in the Veneto Region, located in the North-East of Italy (31). We used 30 sequences (out of 322 suspected cases) analysed in Pacenti et al (31). Sequences were aligned using the Nextstrain measles workflow (52–54). This set of sequences thus corresponded to 9.3% of detected cases. For the analysis, we explore scenarios where:

(i) all infections where detected (corresponding to an infection sequencing ratio of 9.3%)
(ii) half of infections where detected (corresponding to an infection sequencing ratio of 4.7%)

For the measles analysis, we used a threshold c_{max}.for the size of cluster of 10,000. Increasing this value to 50,000 did not impact our estimates.

COVID-19 pandemic in New-Zealand

We analysed 27,565 SARS-CoV-2 sequences from New Zealand downloaded from the GISAID EpiCoV database on December 8th, 2022 (55,56) and curated using the Nextstrain nCoV ingest pipeline (57). Clusters of identical sequences were generated using the approach detailed below and grouped by time period based on the collection date of the earliest sequence.

We estimated the offspring distribution of COVID-19 in New Zealand during the Zero COVID era (April 2020 – July 2021). We assumed that the dispersion parameter k remained constant throughout the period but allowed the reproduction number R to vary between time periods (April-May 2020, June-December 2020, January-April 2021 and May-July 2021). As a baseline scenario, we considered that throughout this period, 80% of infections were detected. Since autochthonous transmission remained extremely limited during this period, it is indeed unlikely that a large fraction of infections was undetected by the surveillance system. As a sensitivity analysis, we also explored scenarios where 50% and 100% of infections were detected. For each time period, the fraction of cases sequenced was estimated as the ratio of the number of sequences collected and of the number of cases (58) reported during this time period.

For this analysis, we used a threshold c_{max}.for the size of cluster of 10,000. Increasing this value to 50,000 did not impact our estimates.

As k estimates may be difficult to interpret, we computed the expected proportion of individuals contributing to 80% of transmission events. This was done for maximum-likelihood estimates of the dispersion parameter and the reproduction numbers across the 4 periods (central estimates) and for the bounds of 95% likelihood profile confidence interval for k (while using maximum likelihood estimates for R).

COVID-19 pandemic in Washington state

We analysed 140,790 SARS-CoV-2 sequences from Washington state (United States of America) downloaded from the GISAID EpiCoV database on December 8th, 2022 (55,56) and curated using the Nextstrain nCoV ingest pipeline (57). As for the New-Zealand analysis, we allocated a date to each cluster of identical sequences based on the collection date of the earliest sequence.

We applied our transmission advantage framework to the following variants: D614G, the Nextstrain clade 20G, Alpha, Delta, Epsilon, Omicron BA.1, Omicron BA.2 and Omicron BA.4/BA.5. For each variant, we arbitrarily defined a time window of analysis (Table S5) and selected the clusters of identical SARS-CoV-2 sequences who started during this period. We then generated the size distribution of clusters of identical sequences for both the variant and non-variant genetic sub-populations (Figure S11). From this, we applied tour transmission advantage inference framework and computed a p-value associated with the statistical test defined by the following null hypothesis:

H_0: There is no difference in the reproduction number of the variant and non-variant.

This was done by accounting for the fraction of cases sequenced in Washington state during these different time periods and exploring different assumptions regarding the fraction of infections detected.

Defining clusters of identical sequences

For each dataset, we computed a pairwise distance matrix between aligned sequences using the *ape* R package (59). If there weren't any missing data (sites) in the sequences, this matrix would directly enable to reconstruct clusters of identical sequences. In practice, this is not the case. We thus defined clusters of identical sequences as maximal groups of sequences for which all sequences were at a null distance

to all other sequences within the cluster. The difference between pairwise distances and clusters of identical sequences is illustrated in Figure S13 in the case of MERS-CoV. The cluster generation was done using the R *igraph* package (60).

Due to the large number of sequences available for SARS-CoV-2, generating a single pairwise genetic distance matrix would be computationally and memory intensive. Instead, we grouped sequences by pango lineage assigned with Nextclade (34,35) and generated a pairwise genetic distance matrix for each pango lineage.

Data and code accessibility

The codes and data used in this paper can be found at https://github.com/blab/size-genetic-clusters. The MERS aligned sequences used in the analysis were directly extracted from the aligned human sequence data available at (51). The GISAID accession numbers associated with the SARS-CoV-2 sequences used in this analysis (both for New-Zealand and Washington state) are provided as a supplementary file. The size distributions of clusters of identical sequences used to run the different analyses are available in the associated GitHub repository. We provide scripts to ingest FASTA files to produce cluster distributions and also scripts to estimate R and k from input cluster distribution.

Author contributions

CTK and TB conceived the study. CTK developed the methods, conducted the analyses, interpreted the results, and wrote the first draft. CTK and TB edited the initial manuscript.

Acknowledgments

We would like to thank James Hadfield for his help on the interpretation of the New Zealand data, John Huddleston, Jennifer Chang, Alli Black and Paolo Bosetti for helpful feedbacks on a first draft and Simon Cauchemez for helpful discussions. We gratefully acknowledge all data contributors, i.e., the Authors and their Originating laboratories responsible for obtaining the specimens, and their Submitting laboratories for generating the genetic sequence and metadata and sharing via the GISAID Initiative, on which this research is based. We also greatly acknowledge authors, alongside their originating and submitting laboratories for generating and submitting the sequences and associated metadata on Genbank. The Genbank accession numbers associated with the measles sequences used in the analysis are detailed in Table S6. A full acknowledgement table for SARS-CoV-2 sequences is available as a supplementary file.

Funding

TB is a Howard Hughes Medical Institute Investigator. This work is supported by NIH NIGMS R35 GM119774 awarded to TB. Most of the analyses were completed using Fred Hutch Scientific Computing resources (NIH grants S10-OD-020069 and S10-OD-028685).

Competing interests

We declare no competing interests.

References

1. Anderson RM, May RM. Infectious diseases of humans: Dynamics and control. London, England: Oxford University Press; 1992. 772 p.

2. Cori A, Ferguson NM, Fraser C, Cauchemez S. A new framework and software to estimate time-varying reproduction numbers during epidemics. Am J Epidemiol. 2013 Nov 1;178(9):1505–12.

3. Wallinga J, Teunis P. Different epidemic curves for severe acute respiratory syndrome reveal similar impacts of control measures. Am J Epidemiol. 2004 Sep 15;160(6):509–16.

4. Cauchemez S, Boelle P-Y, Donnelly CA, Ferguson NM, Thomas G, Leung GM, et al. Real-time estimates in early detection of SARS. Emerg Infect Dis. 2006 Jan;12(1):110–3.

5. Lloyd-Smith JO, Schreiber SJ, Kopp PE, Getz WM. Superspreading and the effect of individual variation on disease emergence. Nature. 2005 Nov 17;438(7066):355–9.

6. Cauchemez S, Boëlle P-Y, Thomas G, Valleron A-J. Estimating in real time the efficacy of measures to control emerging communicable diseases. Am J Epidemiol. 2006 Sep 15;164(6):591–7.

7. Gostic KM, McGough L, Baskerville EB, Abbott S, Joshi K, Tedijanto C, et al. Practical considerations for measuring the effective reproductive number, Rt. PLoS Comput Biol. 2020 Dec;16(12):e1008409.

8. Nishiura H, Yan P, Sleeman CK, Mode CJ. Estimating the transmission potential of supercritical processes based on the final size distribution of minor outbreaks. J Theor Biol. 2012 Feb 7;294:48–55.

9. Blumberg S, Lloyd-Smith JO. Inference of R(0) and transmission heterogeneity from the size distribution of stuttering chains. PLoS Comput Biol. 2013 May 2;9(5):e1002993.

10. Blumberg S, Lloyd-Smith JO. Comparing methods for estimating R0 from the size distribution of subcritical transmission chains. Epidemics. 2013 Sep;5(3):131–45.

11. Campbell F, Strang C, Ferguson N, Cori A, Jombart T. When are pathogen genome sequences informative of transmission events? PLoS Pathog. 2018 Feb;14(2):e1006885.

12. Jombart T, Cori A, Didelot X, Cauchemez S, Fraser C, Ferguson N. Bayesian reconstruction of disease outbreaks by combining epidemiologic and genomic data. PLoS Comput Biol. 2014 Jan;10(1):e1003457.

13. Didelot X, Fraser C, Gardy J, Colijn C. Genomic infectious disease epidemiology in partially sampled and ongoing outbreaks. Mol Biol Evol. 2017 Jan 18;msw075.

14. Grenfell BT, Pybus OG, Gog JR, Wood JLN, Daly JM, Mumford JA, et al. Unifying the epidemiological and evolutionary dynamics of pathogens. Science. 2004 Jan 16;303(5656):327–32.

15. Volz EM, Koelle K, Bedford T. Viral phylodynamics. PLoS Comput Biol. 2013 Mar 21;9(3):e1002947.

16. Bedford T, Greninger AL, Roychoudhury P, Starita LM, Famulare M, Huang M-L, et al. Cryptic transmission of SARS-CoV-2 in Washington state. Science. 2020 Oct 30;370(6516):571–5.

17. Fraser C, Donnelly CA, Cauchemez S, Hanage WP, Van Kerkhove MD, Hollingsworth TD, et al. Pandemic potential of a strain of influenza A (H1N1): early findings. Science. 2009 Jun 19;324(5934):1557–61.

18. Pybus OG, Charleston MA, Gupta S, Rambaut A, Holmes EC, Harvey PH. The epidemic behavior of the hepatitis C virus. Science. 2001 Jun 22;292(5525):2323–5.

19. Lloyd-Smith JO. Maximum likelihood estimation of the negative binomial dispersion parameter for highly overdispersed data, with applications to infectious diseases. PLoS One. 2007 Feb 14;2(2):e180.

20. Waxman D, Nouvellet P. Sub- or supercritical transmissibilities in a finite disease outbreak: Symmetry in outbreak properties of a disease conditioned on extinction. J Theor Biol. 2019 Apr 21;467:80–6.

21. Cori A, Nouvellet P, Garske T, Bourhy H, Nakouné E, Jombart T. A graph-based evidence synthesis approach to detecting outbreak clusters: An application to dog rabies. PLoS Comput Biol. 2018 Dec;14(12):e1006554.

22. Memish ZA, Perlman S, Van Kerkhove MD, Zumla A. Middle East respiratory syndrome. Lancet. 2020 Mar 28;395(10229):1063–77.

23. Breban R, Riou J, Fontanet A. Interhuman transmissibility of Middle East respiratory syndrome coronavirus: estimation of pandemic risk. Lancet. 2013 Aug;382(9893):694–9.

24. Poletto C, Pelat C, Levy-Bruhl D, Yazdanpanah Y, Boelle PY, Colizza V. Assessment of the Middle East respiratory syndrome coronavirus (MERS-CoV) epidemic in the Middle East and risk of international spread using a novel maximum likelihood analysis approach. Euro Surveill [Internet]. 2014 Jun 12;19(23). Available from: http://dx.doi.org/10.2807/1560-7917.es2014.19.23.20824

25. Kucharski AJ, Althaus CL. The role of superspreading in Middle East respiratory syndrome coronavirus (MERS-CoV) transmission. Euro Surveill. 2015 Jun 25;20(25):14–8.

26. Cauchemez S, Nouvellet P, Cori A, Jombart T, Garske T, Clapham H, et al. Unraveling the drivers of MERS-CoV transmission. Proc Natl Acad Sci U S A. 2016 Aug 9;113(32):9081–6.

27. Dudas G, Carvalho LM, Rambaut A, Bedford T. MERS-CoV spillover at the camel-human interface. Elife [Internet]. 2018 Jan 16;7. Available from: http://dx.doi.org/10.7554/elife.31257

28. Lessler J, Salje H, Van Kerkhove MD, Ferguson NM, Cauchemez S, Rodriquez-Barraquer I, et al. Estimating the severity and subclinical burden of Middle East respiratory syndrome Coronavirus infection in the Kingdom of Saudi Arabia. Am J Epidemiol. 2016 Apr 1;183(7):657–63.

29. Bosetti P, Poletti P, Stella M, Lepri B, Merler S, De Domenico M. Heterogeneity in social and epidemiological factors determines the risk of measles outbreaks. Proc Natl Acad Sci U S A. 2020 Dec 1;117(48):30118–25.

30. Glass K, Kappey K, Grenfell BT. The effect of heterogeneity in measles vaccination on population immunity. Epidemiol Infect. 2004 Aug;132(4):675–83.

31. Pacenti M, Maione N, Lavezzo E, Franchin E, Dal Bello F, Gottardello L, et al. Measles virus infection and immunity in a suboptimal vaccination coverage setting. Vaccines (Basel). 2019 Nov 28;7(4):199.

32. Chiew M, Gidding HF, Dey A, Wood J, Martin N, Davis S, et al. Estimating the measles effective reproduction number in Australia from routine notification data. Bull World Health Organ. 2014 Mar 1;92(3):171–7.

33. Du Z, Wang C, Liu C, Bai Y, Pei S, Adam DC, et al. Systematic review and meta-analyses of superspreading of SARS-CoV-2 infections. Transbound Emerg Dis. 2022 Sep;69(5):e3007–14.

34. Aksamentov I, Roemer C, Hodcroft E, Neher R. Nextclade: clade assignment, mutation calling and quality control for viral genomes. J Open Source Softw. 2021 Nov 30;6(67):3773.

35. Nextclade [Internet]. [cited 2023 Feb 9]. Available from: https://clades.nextstrain.org

36. Gaymard A, Bosetti P, Feri A, Destras G, Enouf V, Andronico A, et al. Early assessment of diffusion and possible expansion of SARS-CoV-2 Lineage 20I/501Y.V1 (B.1.1.7, variant of concern 202012/01) in France, January to March 2021. Euro Surveill [Internet]. 2021 Mar;26(9). Available from: http://dx.doi.org/10.2807/1560-7917.ES.2021.26.9.2100133

37. Figgins MD, Bedford T. SARS-CoV-2 variant dynamics across US states show consistent differences in effective reproduction numbers [Internet]. bioRxiv. 2021. Available from: http://dx.doi.org/10.1101/2021.12.09.21267544

38. Volz E, Mishra S, Chand M, Barrett JC, Johnson R, Geidelberg L, et al. Assessing transmissibility of SARS-CoV-2 lineage B.1.1.7 in England. Nature. 2021 May;593(7858):266–9.

39. Davies NG, Abbott S, Barnard RC, Jarvis CI, Kucharski AJ, Munday JD, et al. Estimated transmissibility and impact of SARS-CoV-2 lineage B.1.1.7 in England. Science. 2021 Apr 9;372(6538):eabg3055.

40. Volz E, Hill V, McCrone JT, Price A, Jorgensen D, O'Toole Á, et al. Evaluating the effects of SARS-CoV-2 spike mutation D614G on transmissibility and pathogenicity. Cell. 2021 Jan 7;184(1):64-75.e11.

41. Müller NF, Wagner C, Frazar CD, Roychoudhury P, Lee J, Moncla LH, et al. Viral genomes reveal patterns of the SARS-CoV-2 outbreak in Washington State. Sci Transl Med. 2021 May 26;13(595):eabf0202.

42. Cauchemez S, Hoze N, Cousien A, Nikolay B, Ten Bosch Q. How modelling can enhance the analysis of imperfect epidemic data. Trends Parasitol. 2019 May;35(5):369–79.

43. Ferguson NM, Fraser C, Donnelly CA, Ghani AC, Anderson RM. Public health. Public health risk from the avian H5N1 influenza epidemic. Science. 2004 May 14;304(5673):968–9.

44. Duchene S, Featherstone L, Haritopoulou-Sinanidou M, Rambaut A, Lemey P, Baele G. Temporal signal and the phylodynamic threshold of SARS-CoV-2. Virus Evol. 2020 Jul;6(2):veaa061.

45. Elie B, Selinger C, Alizon S. The source of individual heterogeneity shapes infectious disease outbreaks. Proc Biol Sci. 2022 May 11;289(1974):20220232.

46. Worby CJ, Lipsitch M, Hanage WP. Within-host bacterial diversity hinders accurate reconstruction of transmission networks from genomic distance data. PLoS Comput Biol. 2014 Mar;10(3):e1003549.

47. R Core Team. R: A language and environment for statistical computing [Internet]. R Foundation for Statistical Computing, Vienna, Austria; 2022. Available from: https://www.R-project.org/

48. Ito K, Piantham C, Nishiura H. Estimating relative generation times and reproduction numbers of Omicron BA.1 and BA.2 with respect to Delta variant in Denmark. Math Biosci Eng. 2022 Jun 21;19(9):9005–17.

49. Abbott S, Sherratt K, Gerstung M, Funk S. Estimation of the test to test distribution as a proxy for generation interval distribution for the Omicron variant in England [Internet]. bioRxiv. 2022. Available from: http://dx.doi.org/10.1101/2022.01.08.22268920

50. Annual threat report 2016 [Internet]. European Centre for Disease Prevention and Control. 2017 [cited 2022 Dec 16]. Available from: https://www.ecdc.europa.eu/en/publications-data/annual-threat-report-2016

51. mers-structure: Looking into MERS-CoV dynamics through the structured coalescent lens [Internet]. Github; [cited 2022 Dec 16]. Available from: https://github.com/blab/mers-structure

52. Huddleston J, Hadfield J, Sibley TR, Lee J, Fay K, Ilcisin M, et al. Augur: a bioinformatics toolkit for phylogenetic analyses of human pathogens. J Open Source Softw. 2021 Jan 7;6(57):2906.

53. Hadfield J, Megill C, Bell SM, Huddleston J, Potter B, Callender C, et al. Nextstrain: real-time tracking of pathogen evolution. Bioinformatics. 2018 Dec 1;34(23):4121–3.

54. nextstrain.org/measles [Internet]. [cited 2022 Dec 16]. Available from: https://github.com/nextstrain/measles

55. Shu Y, McCauley J. GISAID: Global initiative on sharing all influenza data – from vision to reality. Euro Surveill [Internet]. 2017 Mar 30;22(13). Available from: http://dx.doi.org/10.2807/1560-7917.es.2017.22.13.30494

56. GISAID - gisaid.org [Internet]. [cited 2023 Feb 9]. Available from: https://gisaid.org/

57. ncov-ingest: A pipeline that ingests SARS-CoV-2 (i.e. nCoV) data from GISAID and Genbank, transforms it, stores it on S3, and triggers Nextstrain nCoV rebuilds [Internet]. Github; [cited 2023 Feb 9]. Available from: https://github.com/nextstrain/ncov-ingest

58. COVID-19 data portal [Internet]. [cited 2023 Feb 9]. Available from: https://www.stats.govt.nz/experimental/covid-19-data-portal

59. Paradis E, Schliep K. ape 5.0: an environment for modern phylogenetics and evolutionary analyses in R. Bioinformatics. 2019 Feb 1;35(3):526–8.

60. Csardi G, Nepusz T. The Igraph Software Package for Complex Network Research. InterJournal. 2005 Nov;Complex Systems.